PAPER

A multilevel sampling algorithm for locating inhomogeneous media

To cite this article: Keji Liu and Jun Zou 2013 *Inverse Problems* **29** 095003

View the article online for updates and enhancements.

A multilevel sampling algorithm for locating inhomogeneous media

Keji Liu and Jun Zou

Department of Mathematics, The Chinese University of Hong Kong, Shatin, Hong Kong

E-mail: kjliu@math.cuhk.edu.hk and zou@math.cuhk.edu.hk

Abstract
In the reconstruction process of unknown multiple scattering objects in inverse medium scattering problems, the first important step is to effectively locate some approximate domains that contain all inhomogeneous media. Without such an effective step, one may have to take a computational domain of a size that is much larger than the actual sizes of all scattering objects, thus resulting in huge additional computational effort. In this work, we propose a simple and efficient multilevel reconstruction algorithm to help locate an accurate position and the shape of each inhomogeneous medium. Then, other existing effective but computationally more demanding reconstruction algorithms may be applied in these initially located computational domains to achieve more accurate locations and shapes of the scatterer and the contrast values over each medium domain. The new algorithm exhibits several strengths: robustness against noise, requiring fewer incidences, fast convergence, flexibility to deal with scatterers of special shapes and advantages in computational complexity.

(Some figures may appear in colour only in the online journal)

1. Introduction

In this paper, we are concerned with numerical identifications of inhomogeneous medium scatterers by scattered fields. The inverse scattering problem can find wide applications in medicine, geophysics and biological studies. A large variety of numerical reconstruction methods are available in the literature, such as the time-reversal multiple signal classification (MUSIC) method [9, 15], the contrast source inversion (CSI) method [1, 17–19], the continuation method [2], the subspace-based optimization method [4, 5], the linear sampling or probing methods (LSM) [7, 12, 13, 16, 20], the parallel radial bisection method [14], etc. In order to carry out any of these methods for the reconstruction of unknown multiple scattering objects, the first important step is to effectively locate some approximate domains that contain all scattering objects. Without such an effective step, one may have to take a computational domain of a size that is much larger than the actual sizes of all scattering objects. In particular, when multiple separated objects are present, and at least two of them are far away from each

other, then one may need to set an initial computational/sampling domain to be sufficiently large in order to ensure a safe covering of all scattering objects, easily selecting a domain with an area or a volume of 30 or 40 times as large as the actual region required to cover all inhomogeneous media. A much larger computational domain results usually in a huge additional computational effort for the entire numerical reconstruction process, considering the severe ill-posedness and strong nonlinearity of inverse medium scattering problems.

So it is of great significance for the reconstruction process of an inverse medium problem to have an effective step that helps locate the initial regions covering each of the scattering objects. In addition, this first step should be less expensive computationally and easy to implement numerically. It is mostly challenging to realize this task and to provide an acceptable initial location of each scattering object at the same time. A direct sampling method was proposed recently in [8] for the purpose. The algorithm is computationally very cheap as it involves computing only the inner product of the scattered field with fundamental solutions located at sampling points. In this paper, we will propose a new algorithm for the purpose, and it is completely different from the one in [8]. This new algorithm is an iterative one, and also very cheap; only three matrix–vector multiplications are needed at each iteration, without any matrix inversion or solutions of linear systems involved. Most interestingly, the algorithm can first separate all disjoint inhomogeneous medium objects quickly, usually in a few iterations, then refine its approximation successively and finally provide a good approximate domain for each separated object.

It is worth mentioning that the multilevel algorithm to be presented here is essentially different in nature from the multilevel linear sampling method developed in [12]: the new method is much less sensitive to the so-called cut-off values, it works with much fewer incident fields, and it does not need to solve an ill-posed far-field equation at every sampling point. In addition, the new algorithm is robust against noise in the data. More importantly, unlike most existing methods, the new method does not involve any optimization process or matrix inversions, so it can be viewed as a direct sampling method. Another nice feature of the new algorithm is that it is self-adaptive, that is, at each iteration it can remedy the possible errors from the previous iterations. With an effective initial location of each scattering object, we may then apply any existing efficient but computationally more demanding methods, e.g., the methods in [2, 5, 17, 18], for further refinement of the estimated location and shape of each scattering object as well as for the recovery of the contrast profiles of different media. Finally, we would like to emphasize that the new multilevel method aims only at weak scatterers. It is well known that it is of great challenge to numerically reconstruct strong scatterers (i.e., scatterers with both high contrast values and large electrical sizes), since the wave behaviors inside and among them are highly complex. So far there is still no efficient method that can successfully tackle this problem, neither can our multilevel algorithm deal with it. However, considering the fact that the LSM does not need to involve the wave interactions inside and among scatterers, it may still be possible to locate strong scatterers if the number of incidences is sufficient.

2. Problem description

Consider an inverse scattering problem where the scatterer Ω, possibly consisting of several separated disjoint components, is located in a homogeneous background medium $\mathbb{R}^d$ ($d = 2, 3$). We assume that the scattered obstacles are illuminated successively by a number of plane wave incident fields $u_j^{\text{inc}}(\boldsymbol{x})$, $j = 1, 2, \ldots, N_i$. For each plane wave incidence, the scattered field $u_j^{\text{sca}}(\boldsymbol{x}_q^s)$ is measured by the receivers at locations $\boldsymbol{x}_1^s, \ldots, \boldsymbol{x}_{N_s}^s$; see figure 1 for the incidences and receivers located on a circle S.
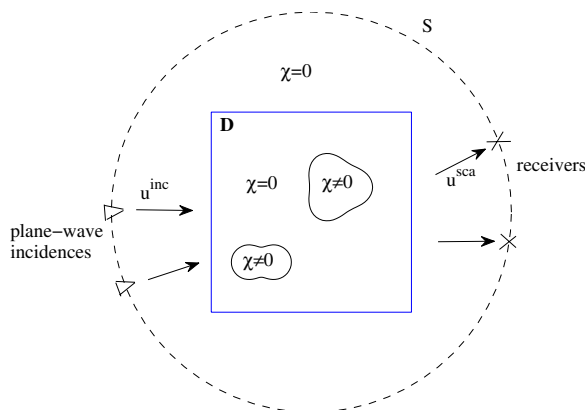
Figure 1. Geometrical model of the scattering problem.

The inverse scattering problem is to determine the contrast function or index of refraction, $\chi(\boldsymbol{x})$ for any point $\boldsymbol{x}$ varying in the scatterer Ω, given a set of scattering data $u_j^{\mathrm{sca}}(\boldsymbol{x}_q^s)$. The contrast χ has a very important property, i.e., it vanishes outside the scattering objects. For each incident field u_j^{inc}, the total field u_j satisfies the Helmholtz equation [7],

$$\Delta u_j(\boldsymbol{x}) + k^2(\chi(\boldsymbol{x}) + 1)u_j(\boldsymbol{x}) = 0, \quad \boldsymbol{x} \in \mathbb{R}^d, \tag{2.1}$$

where k is the wavenumber of the homogeneous background medium. The total field u_j can be represented by the integral equation [7],

$$u_j(\boldsymbol{x}) = u_j^{\mathrm{inc}}(\boldsymbol{x}) + k^2 \int_\Omega g(\boldsymbol{x}, \boldsymbol{x}')\chi(\boldsymbol{x}')u_j(\boldsymbol{x}')\, \mathrm{d}v(\boldsymbol{x}'), \tag{2.2}$$

where $g(\boldsymbol{x}, \boldsymbol{x}')$ is the Green function of the homogeneous background medium,

$$g(\boldsymbol{x}, \boldsymbol{x}') = \begin{cases} \dfrac{\mathrm{i}}{4} H_0^{(1)}(k|\boldsymbol{x} - \boldsymbol{x}'|) & \text{for} \quad d = 2, \\[2mm] \dfrac{\mathrm{e}^{\mathrm{i}k|\boldsymbol{x} - \boldsymbol{x}'|}}{4\pi |\boldsymbol{x} - \boldsymbol{x}'|} & \text{for} \quad d = 3, \end{cases}$$

where $H_0^{(1)}$ is the zero-order Hankel function of a first kind. We note that the total field u_j may stand for the acoustic pressure in an acoustic scattering problem, or for the electric field vector in an electromagnetic scattering, or for the particle-velocity vector in an elastodynamic scattering. The scattered field is measured on the boundary S of a domain, which is sitting outside the scatterer Ω. We introduce a sampling domain **D** that completely cover the scatterer Ω. As the contrast function χ vanishes outside Ω, with the help of (2.2), we can write the scattered field as

$$u_j^{\mathrm{sca}}(\boldsymbol{x}) = u_j(\boldsymbol{x}) - u_j^{\mathrm{inc}}(\boldsymbol{x}) = k^2 \int_D g(\boldsymbol{x}, \boldsymbol{x}')\chi(\boldsymbol{x}')u_j(\boldsymbol{x}')\, \mathrm{d}v(\boldsymbol{x}'), \quad \boldsymbol{x} \in \mathrm{S}. \tag{2.3}$$

For the sake of convenience, we shall often introduce the contrast source function

$$w_j(\boldsymbol{x}) = \chi(\boldsymbol{x})u_j(\boldsymbol{x}), \quad \boldsymbol{x} \in \mathrm{D}. \tag{2.4}$$

Then, we can write (2.2) and (2.3) in the following more compact forms:

$$w_j(\boldsymbol{x}) = \chi(\boldsymbol{x})u_j^{\mathrm{inc}}(\boldsymbol{x}) + \chi(\boldsymbol{x})(G_D w_j)(\boldsymbol{x}), \quad \boldsymbol{x} \in \mathrm{D} \tag{2.5}$$

and

$$u_j^{\mathrm{sca}}(\boldsymbol{x}) = (G_S w_j)(\boldsymbol{x}), \quad \boldsymbol{x} \in \mathrm{S}, \tag{2.6}$$

where G_D and G_S are the two integral operators given by

$$(G_D w)(\boldsymbol{x}) = k^2 \int_D g(\boldsymbol{x}, \boldsymbol{x}') w(\boldsymbol{x}') \, \mathrm{d}v(\boldsymbol{x}') \quad \forall \boldsymbol{x} \in \mathrm{D},$$

$$(G_S w)(\boldsymbol{x}) = k^2 \int_D g(\boldsymbol{x}, \boldsymbol{x}') w(\boldsymbol{x}') \, \mathrm{d}v(\boldsymbol{x}') \quad \forall \boldsymbol{x} \in \mathrm{S}.$$

Equations (2.5) and (2.6) will be the two fundamental equations for our proposed multilevel initialization algorithm.

3. Approximate contrast source by backpropagation

We can easily see that the support of the contrast source function $w = \chi u$ describes the exact locations and geometries of all the inhomogeneous media, which generate the scattered field u^{sca}. The aim of this work is to propose a fast and less expensive algorithm that can help locate all the inhomogeneous media and provide good initial guesses for some computationally more demanding iterative algorithms to find more accurate locations and shapes of all the inhomogeneous media and the approximations of the contrast function χ.

Our algorithm will rely on the approximate contrast source obtained by backpropagation. Backpropagation is widely used in inverse medium scatterings; see [11, 18] and the references therein. In this section, we shall give a rigorous mathematical explanation of the approximate contrast source by backpropagation. Let $(\cdot, \cdot)_{L^2(S)}$ and $(\cdot, \cdot)_{L^2(D)}$ be the scalar products, respectively, in $L^2(S)$ and $L^2(D)$, and $G_s^* \colon L^2(S) \to L^2(D)$ be the adjoint of the operator $G_s \colon L^2(D) \to L^2(S)$. G_s^* is called the backpropagation operator and given by

$$(G_S^* w)(\boldsymbol{x}) = k^2 \int_S \overline{g(\boldsymbol{x}, \boldsymbol{x}')} w(\boldsymbol{x}') \, \mathrm{d}s(\boldsymbol{x}') \quad \forall \boldsymbol{x} \in \mathrm{D}.$$

We shall need the following backpropagation subspace of $L^2(D)$,

$$V_b = \mathrm{span}\{G_s^* u^{\mathrm{sca}}\},$$

which is formed by all the fields generated by the backpropagation G_s^* on the scattered data u^{sca}. It follows from (2.6) that

$$u^{\mathrm{sca}}(\boldsymbol{x}) = (G_S w)(\boldsymbol{x}), \quad \boldsymbol{x} \in \mathrm{S}. \tag{3.1}$$

The backpropagation is to seek a best approximate solution w_b to the equation (3.1) in the backpropagation subspace V_b, namely

$$||u^{\mathrm{sca}} - G_s w_b||^2_{L^2(S)} = \min_{v_b \in V_b} ||u^{\mathrm{sca}} - G_s v_b||^2_{L^2(S)}. \tag{3.2}$$

It is easy to see that the solution w_b to (3.2) solves the variational system,

$$(u^{\mathrm{sca}} - G_s w_b, G_s v_b)_{L^2(S)} = 0 \quad \forall\, v_b \in V_b, \tag{3.3}$$

or equivalently,

$$(G_s w_b, G_s v_b)_{L^2(S)} = (G_s^* u^{\mathrm{sca}}, v_b)_{L^2(D)} \quad \forall\, v_b \in V_b. \tag{3.4}$$

As $w_b, v_b \in V_b$, we can write

$$w_b = \lambda \, G_s^* u^{\mathrm{sca}}, \quad v_b = \mu \, G_s^* u^{\mathrm{sca}}, \tag{3.5}$$

for some constants λ and μ. Substituting the two expressions into (3.4), we obtain

$$\lambda = \frac{||G_s^* u^{\mathrm{sca}}||^2_{L^2(D)}}{||G_s G_s^* u^{\mathrm{sca}}||^2_{L^2(S)}}, \tag{3.6}$$

which gives the approximate contrast source by backpropagation,

$$w_b = \frac{||G_s^* u^{\mathrm{sca}}||^2_{L^2(D)}}{||G_s G_s^* u^{\mathrm{sca}}||^2_{L^2(S)}} \, G_s^* u^{\mathrm{sca}}. \tag{3.7}$$

4. A multilevel sampling algorithm

In this section, we propose a fast multilevel sampling algorithm to find the locations and geometric shapes of all the inhomogeneous media, which are described by the contrast function χ in (2.1). The algorithm proceeds iteratively, and carries out two important steps at each iteration based on the two fundamental equations (2.5) and (2.6), namely the state and field equations, respectively. In the first step, we apply the backpropagation technique to compute an approximate contrast source w_j corresponding to each incident u_j^{inc} ($j = 1, 2, \ldots, N_i$). It follows from (3.7) that this approximation is given by

$$w_j = \frac{||G_S^* u_j^{\text{sca}}||_{L^2(D)}^2}{||G_S G_S^* u_j^{\text{sca}}||_{L^2(S)}^2} \, G_S^* u_j^{\text{sca}}, \quad j = 1, 2, \ldots, N_i. \tag{4.1}$$

With these approximate contributions w_j of the exact contrast source w corresponding to each incident u_j^{inc}, we approximate the contrast χ pointwise by minimizing the residual equation corresponding to the state equation (2.5), namely

$$\min_{\chi(\boldsymbol{x}) \in \mathbf{R}^1} \sum_{j=1}^{N_i} \left| \big(\chi u_j^{\text{inc}} - w_j + \chi G_D w_j \big)(\boldsymbol{x}) \right|^2, \tag{4.2}$$

which yields an explicit formula to compute an approximate contrast value $\chi(\boldsymbol{x})$ at every point $\boldsymbol{x} \in D$ when an approximate contrast source w_j is available,

$$\chi(\boldsymbol{x}) = \text{Re} \left(\frac{\sum_{j=1}^{N_i} w_j(\boldsymbol{x}) \, \overline{(u_j^{\text{inc}} + G_D w_j)(\boldsymbol{x})}}{\sum_{j=1}^{N_i} |(u_j^{\text{inc}} + G_D w_j)(\boldsymbol{x})|^2} \right), \tag{4.3}$$

where the overbear denotes the complex conjugate and Re means taking the real part of a complex number. We remark that it may not be always effective to consider only the real part as in (4.3), especially for those lossy scatterers whose contrast values may have a small real part but a large imaginary part. In those cases, we may take the absolute value of the reconstructed contrast function in (4.3).

Clearly both (4.1) and (4.3) are rather crude, in general, and may provide rather poor approximations for the exact contrast source w and contrast profile χ [6]. But, as will be seen, when we combine these two poor approximations in a novel manner with some multilevel technique, it generates a very efficient and robust algorithm for locating an accurate position and the shape of each inhomogeneous medium.

We emphasize that the unique goal of this work is to develop a simple and less expensive algorithm that can help to locate an approximate position and shape of each inhomogeneous medium, but it is not designed for an accurate approximation of the contrast values of the inhomogeneous media.

The basic idea that motivates our algorithm is based on the following simple observation. We know that the exact contrast function $\chi(\boldsymbol{x})$ vanishes outside the scatterer Ω, so its support provides the location and shape of the scatterer Ω, which is formed by all the inhomogeneous media. This observation, along with the previous two explicit evaluation formulae (4.1) and (4.3) and a novel multilevel technique, forms the foundation of our new multilevel sampling algorithm.

For the description of the algorithm, we first introduce two new concepts, *the smallest distance* and *the first gap interval* with index M. For a given finite positive non-decreasing sequence, $\{\chi_1, \chi_2, \ldots, \chi_m\}$, *its smallest distance* is the positive smallest one among all the distances between two neighboring elements, namely $dist(\chi_i, \chi_{i+1})$, $i = 1, 2, \ldots, m-1$. Among all these $m-1$ distances, if there exists some j such that $2 \leqslant j \leqslant m-1$ and the distance

$dist(\chi_j, \chi_{j+1})$ is M times larger than *the smallest distance* of the sequence $\{\chi_1, \chi_2, \ldots, \chi_j\}$, then $[\chi_j, \chi_{j+1}]$ is called *a gap interval*. The first such interval is called *the first gap interval*.

Now we are ready to state our new algorithm.

Multilevel sampling algorithm.

(1) Choose a sampling domain **D** that contains the scatterer Ω.
Select a uniform (coarse) mesh on **D**, consisting of square (2D) or cubic (3D) elements; write the mesh as D_0.
Select a tolerance ε and an index M; set an initial cut-off value $c_0 := 0$ and $k := 1$.

(2) Compute an approximate value of the contrast $\chi_k(\boldsymbol{x})$ at each grid point $\boldsymbol{x} \in D_{k-1}$, using the formulae (4.1) and (4.3). Then do the following:

    (2.1) Order all the values of $\chi_k(\boldsymbol{x})$ satisfying $\chi_k(\boldsymbol{x}) \geqslant c_{k-1}$ into a non-decreasing sequence. Find *the first gap interval* of the sequence with index M.
Choose the right endpoint of *this first gap interval* with index M as the next cut-off value c_k.

    (2.2) If $\chi_k(\boldsymbol{x}) \geqslant c_k$ at a grid point $\boldsymbol{x}$, select all the grid points of the elements which share $\boldsymbol{x}$ as one of their vertices.
Remove all the grid points in D_{k-1}, which are not selected.
Update D_{k-1} by all those selected grid points.

(3) If $|c_k - c_{k-1}| \leqslant \varepsilon$, set $D_k := D_{k-1}$ and go to step 4;
otherwise refine the mesh D_{k-1} to obtain D_k; set $k := k + 1$ and go to step 2.

(4) Output all grid points in D_k for the domains of all inhomogeneous media.

We would like to make an important remark about the index M used in the multilevel sampling algorithm. This index is basically a limit value to help separate numerically the contrast values of the homogeneous background medium from those of the inhomogeneous media. Its motivation lies in the fact that the exact contrast value of the homogeneous background medium is 0, while the ones for the inhomogeneous media are usually significantly larger in magnitude since we are comparing 0 (homogeneous medium) and non-zero (inhomogeneous media), so it is reasonable to locate the interval where the contrast values have the first expected large jump (namely the first gap interval with index M, and M is to measure the jump), then classify the grid points with the small contrast values (less than the cut-off value, i.e., the right endpoint of the first gap interval) as the background medium region, and the grid points with the larger contrast values (larger than the cut-off value) as the inhomogeneous medium regions.

The effectiveness of the multilevel algorithm is not so sensitive to the choice of the index M and mostly we can take it in the range 80–120. For all the numerical experiments we show in the following section, we have simply fixed M to be 100.

We can easily see that the above multilevel sampling algorithm does not involve any optimization process or matrix inversions, and its major cost is to update the contrast values using the explicit formulae (4.1) and (4.3) at each iteration, and the computational sampling domain D_k shrinks as the iteration goes. So the algorithm is rather simple and less expensive. In addition, as the cut-off values are basically to distinguish the homogeneous background medium where $\chi(\boldsymbol{x})$ vanishes and the inhomogeneous media where $\chi(\boldsymbol{x})$ should be essentially different from 0 (it can be small, say 0.3, which is still relatively large in magnitude when compared with zero), so our cut-off values are rather easy to choose and insensitive to the size and physical features of scatterers. In fact, the cut-off value can start simply with zero, then it is updated automatically with the iteration. As we shall see from numerical examples

in the following section, the algorithm works well with few incidents, even with one; and it is self-adaptive, namely it can recover some elements that have been removed in the previous iterations due to computational errors. In terms of these aspects, this new multilevel sampling algorithm outperforms the popular linear sampling methods [16], including the improved multilevel variant [12].

Remark 4.1. Many existing refinement techniques can be used for the mesh refinement required in step 3. In all our numerical experiments, we have adopted the simple bisection technique, namely, we divide each square element into four equal sub-squares in 2D, or divide each cubic element into eight equal smaller cubes in 3D.

5. Numerical simulations

In this section, we present several examples to verify the effectiveness and robustness of the newly proposed multilevel sampling algorithm.

We first use the state and field equations (2.5) and (2.6) (more accurately, their discrete forms (A.1) and (A.2)) to generate the synthetic scattered field data. To do so, equation (A.1) is solved first for the field w_j for each incident field u_j^{inc}, then the scattered data u_j^{sca} is computed from (A.2). Sufficiently fine meshes are used to ensure reliable accuracies of the synthetic data.

Now we list the parameters that are used in our numerical simulations. The wave number k and wave length λ are taken to be $k = 2\pi$ and $\lambda = 1$. For two dimensions, the number of incidences and receivers are set to be $N_i = 6$ and $N_s = 30$, respectively, and the incident wave directions are evenly distributed on the unit circle, while the receivers are equally distributed on the circle of radius 5λ. For three dimensions, the number of incidences and receivers are set to be $N_i = 20$ and $N_s = 182$, respectively, the incident wave directions are evenly distributed on the unit sphere, while the receivers are equally distributed on the surface of the sphere of radius 5λ. The index M of the first gap interval and the tolerance parameter ε are chosen to be 100 and 10^{-3}, respectively. In the two-dimensional numerical simulations, the mesh refinement during the multilevel algorithm is carried out based on the simple bisection rule, namely each square element is divided into four equal subsquares, so we have $h_k = 0.4\lambda/2^k$, where k is the kth refinement, and h_0 and h_k are, respectively, the mesh sizes of the initial mesh and the mesh after the kth refinement. Moreover, random noises are added to the exact scattering data in the following form:

$$u_j^{\text{sca}}(\boldsymbol{x}) := u_j^{\text{sca}}(\boldsymbol{x})[1 + \xi(r_{1,j}(\boldsymbol{x}) + \mathrm{i}r_{2,j}(\boldsymbol{x}))], \quad j = 1, 2, \ldots, N_i,$$

where $r_{1,j}(\boldsymbol{x})$ and $r_{2,j}(\boldsymbol{x})$ are two random numbers varying between -1 and 1, and ξ corresponds to the level of the noise, which is usually taken to be 10% unless specified otherwise. All the programs in our experiments are written in MATLAB and run on a 2.83 GHz PC with 4GB memory.

5.1. Two-dimensional reconstructions

Example 1. This example shows a scatterer Ω consisting of two squares of side length 0.3λ, located, respectively, at $(-0.3\lambda, -0.3\lambda)$ and $(0.3\lambda, 0.3\lambda)$, with their contrast values being 1 and 2, respectively; see the two red squares in figure 3(a). We take the sampling domain $\mathbf{D} = [-1.2\lambda, 1.2\lambda] \times [-1.2\lambda, 1.2\lambda]$, which is quite large compared to the scatterer Ω, with an area 64 times the area of one scatterer component. More importantly, we see that these two small objects are quite close to each other.
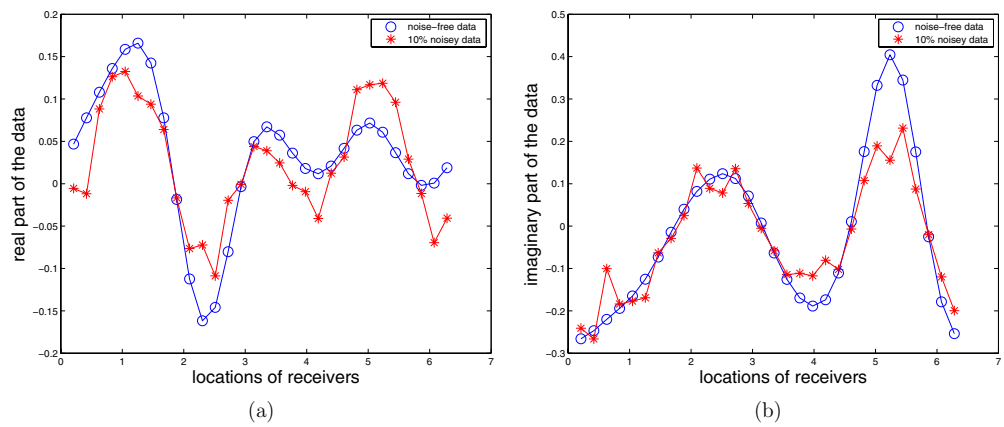
Figure 2. Comparisons of the noise-free data (blue circles) and the data with 10% noise (red stars) for example 1: the real part (a) and imaginary part (b) on the circle of radius 5, with the x-axis representing angles from 0 to 2π.
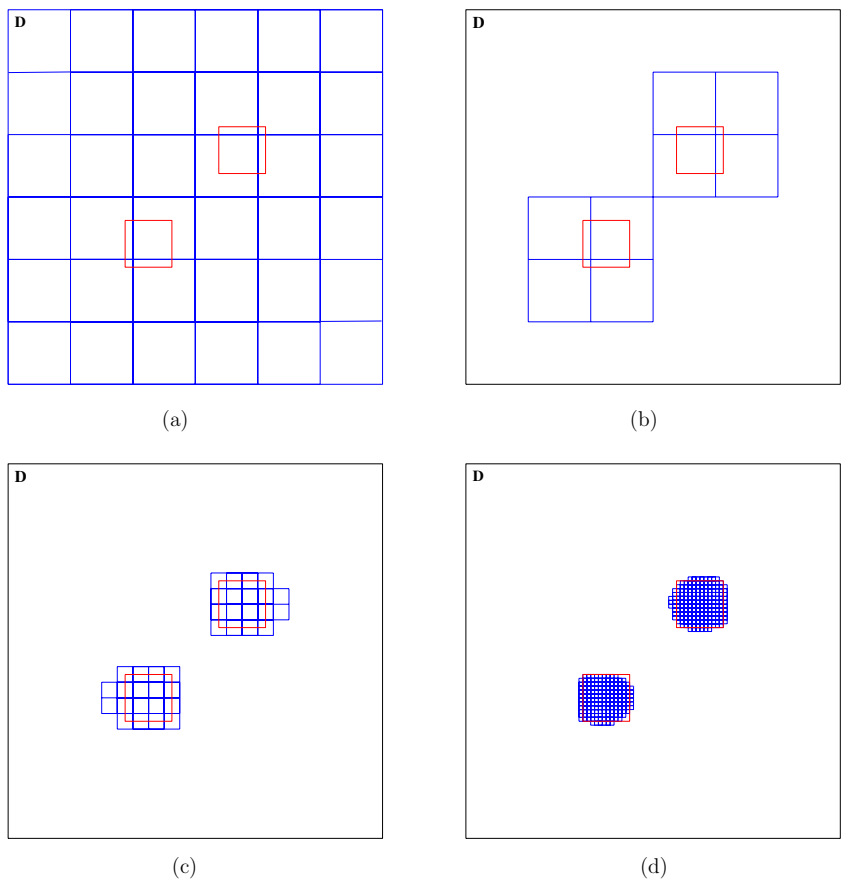

Figure 3. (a) The initial (coarse) mesh on the sampling domain for example 1; (b)–(d) Reconstructions at the first, third and fifth iterations.
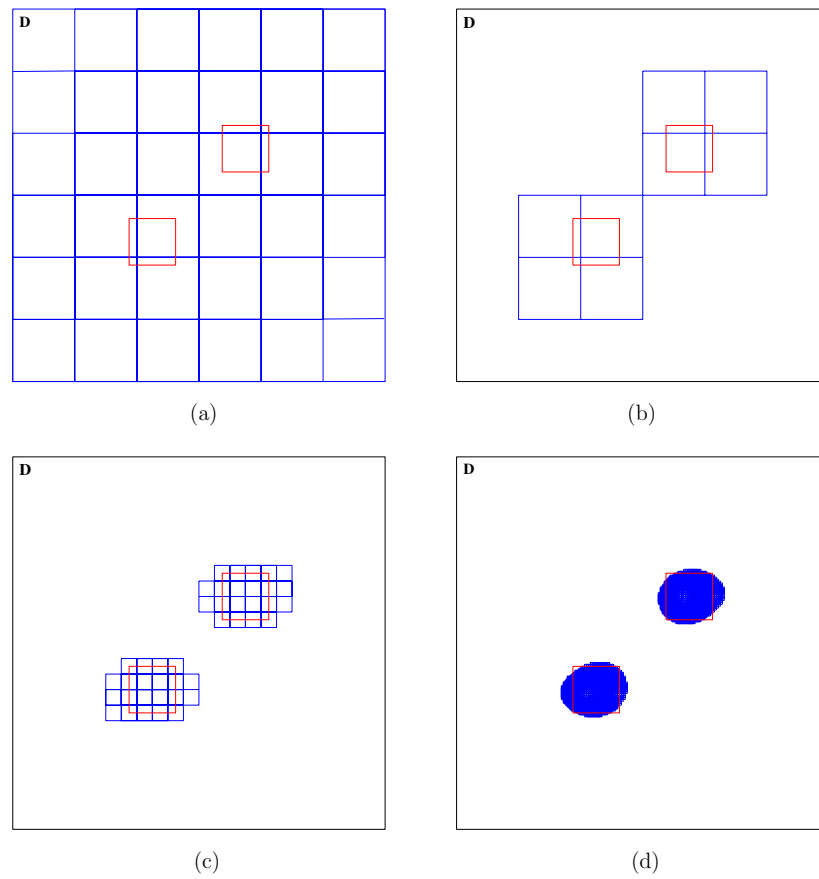
Figure 4. (a) The initial (coarse) mesh on the sampling region for example 2; (b)–(d) Reconstructions at the first, third and sixth iterations.

Table 1. Information about the grid points at each iteration for example 1.

Iteration	1	2	3	4	5
Number of removed grid points	32	18	41	64	59
Number of remaining grid points	17	31	56	118	401
Number of total grid points	49	49	97	182	460

We first show some figures to compare the exact data with the noisy data. When the exact data is polluted with 10% noise, and 30 receivers are used to measure the data corresponding to one incidence, the exact and noisy data are shown in figure 2(a) for the real part of the data, and figure 2(b) for the imaginary part.

The numerical reconstructions are shown in figures 3(b)–(d), respectively, for the first, third and fifth iterations. One can observe from the figures that the algorithm converges very fast and provides quite accurate locations of the two medium components in only five iterations. Moreover, we can see an important advantage of the algorithm, i.e., it can separate the disjoint medium components quickly. One can find more detailed behavior of the algorithm from table 1, which lists the number of grid points that remained or were removed after each iteration.
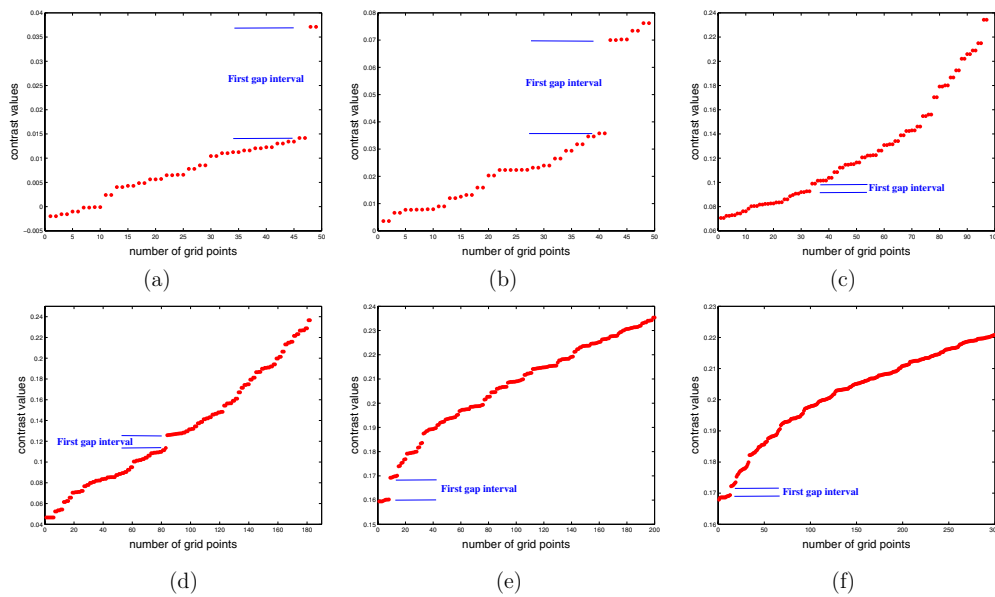
Figure 5. The reconstructed contrast values and the first gap intervals of the first six iterations for example 2.

Table 2. Information about the grid points at each iteration for example 2.

Iteration	1	2	3	4	5	6
Number of removed grid points	32	18	33	84	13	10
Number of remaining grid points	17	31	64	98	452	1604
Number of total grid points	49	49	97	182	465	1614

Example 2. This example is the same as example 1, except that the contrast values of the two medium components are now variable functions, namely

$$\chi(x, y) = \sin \frac{\pi(10|x| - 1.5)}{3} \sin \frac{\pi(10|y| - 1.5)}{3}.$$

The numerical reconstructions are shown in figures 4(b)–(d) for the first, third and sixth iterations. Again, we observe from the figures that the algorithm converges fast, provides very satisfactory locations of the two medium components in only six iterations, and can separate the disjoint medium components quickly.

For a better understanding of the first gap interval, we present in figure 5 the reconstructed contrast values of the remaining grid points and the first gap intervals obtained in the first six iterations. For the plots of the fifth and sixth iterations we have selected only the first 200 and 300 grid points (in a non-decreasing order as the algorithm did), otherwise the points are too many to show in one plot, and the first gap intervals are also difficult to see. As we observe from figure 5(f) that there is nearly no first gap interval at iteration 6, indicating that the remaining grid points are nearly all inhomogeneous media when the algorithm converges.

To see the more detailed behavior of the algorithm in terms of grid points, we have listed in table 2 the number of grid points that remained or were removed after each iteration.

Example 3. This example considers a scatterer Ω of a thin annulus with the inner and outer radii being 0.3λ and 0.5λ, respectively, and centered at the origin. The contrast value $\chi(x)$ is
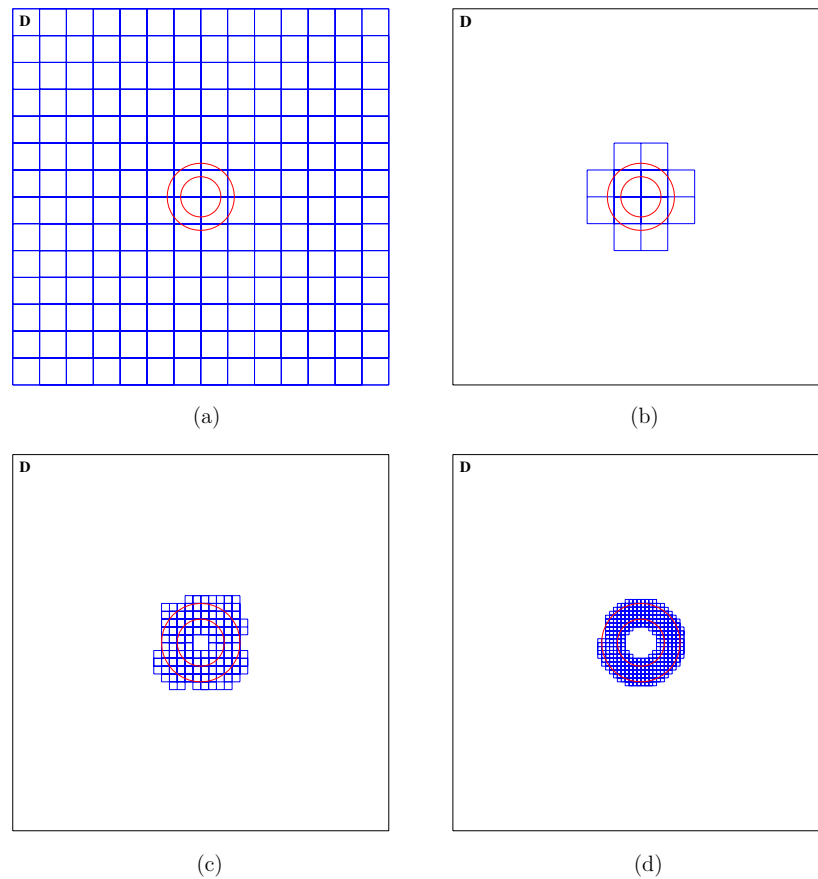
Figure 6. (a) The initial (coarse) mesh on the sampling region for example 3; (b)–(d) Reconstructions at the first, third and fourth iterations.

Table 3. Information about the grid points at each iteration for example 3.

Iteration	1	2	3	4
Number of removed grid points	204	20	37	76
Number of remaining grid points	21	45	111	303
Number of total grid points	225	65	148	379

2 inside the thin annulus. The sampling domain **D** is taken to be a square of side length with 5.6λ, as shown in figure 6(a).

It is easy to see the sampling domain **D** has an area about 62 times as large as the annulus, and the annulus has a very thin thickness, i.e., 0.2λ. The numerical reconstructions are shown in figures 6(b)–(d) for the first, third and fourth iterations. As for the previous two examples, the reconstructions are quite satisfactory and accurate locations for the scatterer can be achieved. Table 3 gives more detailed information about the number of grid points that remained or were removed after each iteration of the multilevel algorithm.

Example 4. This example considers a scatterer Ω of the Austria profile with two cylinders of radii 0.2λ and the ring of the inner and outer radii being 0.3λ and 0.6λ, respectively. The
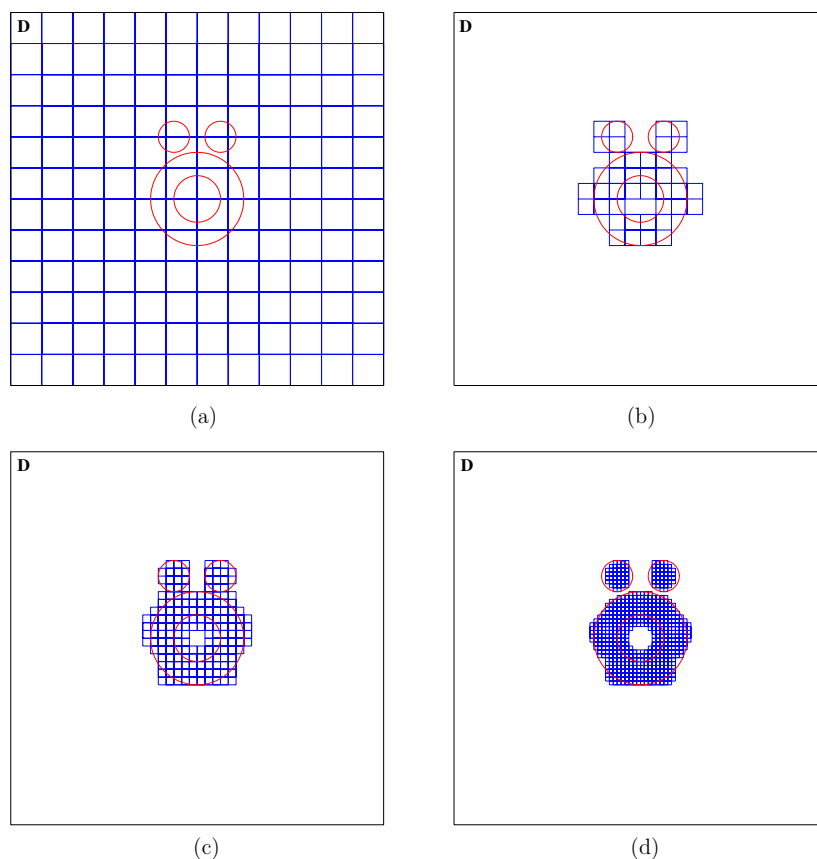
11

Figure 7. (a) The initial (coarse) mesh on the sampling region for example 4; (b)–(d) Reconstructions at the second, third and fourth iterations.

contrast value $\chi(x)$ is set to 1 inside the Austria. The sampling domain **D** is taken to be a square of side length with 4.8λ, as shown in figure 7(a).

It is easy to see that the sampling domain **D** has an area about 21 times as large as the Austria profile, and the annulus has a very thin thickness, i.e., 0.3λ. The numerical reconstructions are shown in figures 7(b)–(d) for the second, third and fourth iterations. As for the previous three examples, the reconstructions are quite satisfactory and accurate locations for the scatterer are achieved. Moreover, the algorithm can separate the top two small circles from the annulus, although the distances between them are rather small.

As we have emphasized earlier, a good feature of the multilevel algorithm is its self-adaptiveness. We may see from figure 7 that the result from the second iteration (figure 7(b)) has excluded four subregions (two on the top middle and two near the bottom left and right) of the inhomogeneous media, but they are basically recovered at the next iteration (figure 7(c)). So the self-adaptiveness of the algorithm may remedy some possible errors from the previous iterations at a current step.

Example 5. In this example, we test the algorithm with partial data to reconstruct an inhomogeneous scatterer. We use only two incidences at directions, $d = \frac{\sqrt{2}}{2}(1, 1)$ and $\frac{\sqrt{2}}{2}(-1, 1)$, and nine receivers evenly distributed on the top half of the circle of radius 5λ. The
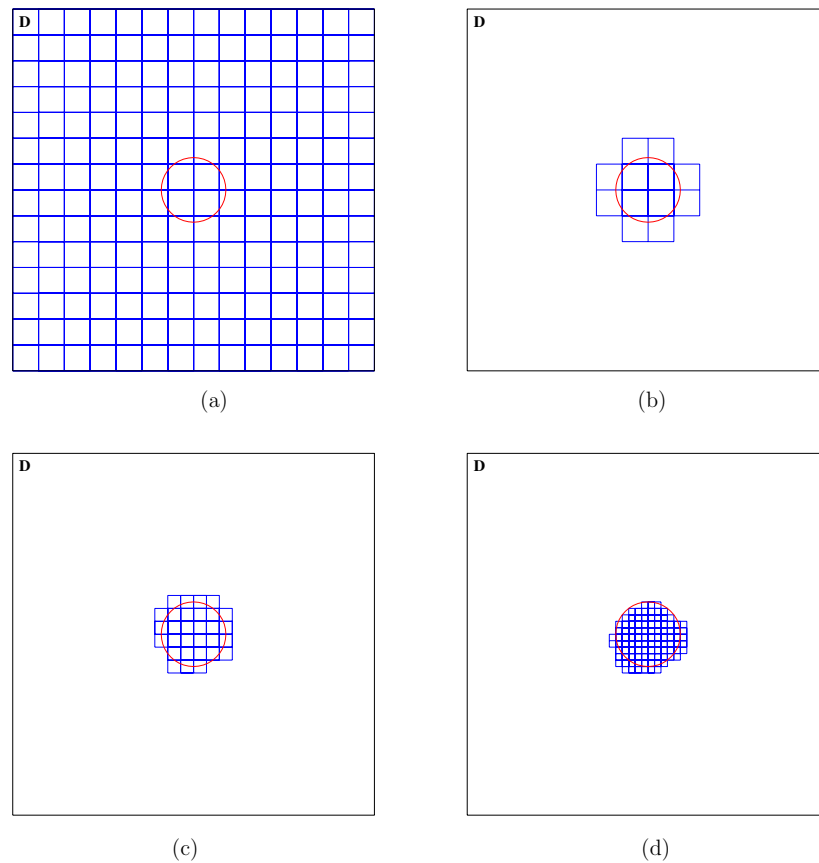
Figure 8. (a) The initial (coarse) mesh on the sampling region for example 5; (b)–(d) Reconstructions at the first three iterations.

sampling domain **D** is selected to be a square of side length with 5.6λ, as shown in figure 8(a). The inhomogeneous medium is a small circle of radius 0.5 with a contrast value 1, and the result is shown in figure 8. We can compute that the sampling domain **D** has an area about 40 times as large as the small circular profile.

As one may see, the location of the inhomogeneous medium is basically accurate, with the top boundary quite well reconstructed but the bottom boundary less accurately reconstructed. The reconstructions seem reasonable as we have only two incidences and measurements on the top part.

5.2. Reconstruction for the contrast function χ

Many numerical methods are available in the literature for reconstructing the contrast profile function χ. These methods are usually more refined and accurate than the new multilevel method for recovering both the geometric shapes and the contrast functions of the inhomogeneous media, but they are usually more complicated technically and much more demanding computationally, as they mostly involve nonlinear optimizations and matrix inversions. Without a reasonably good initial location for each inhomogeneous medium, we
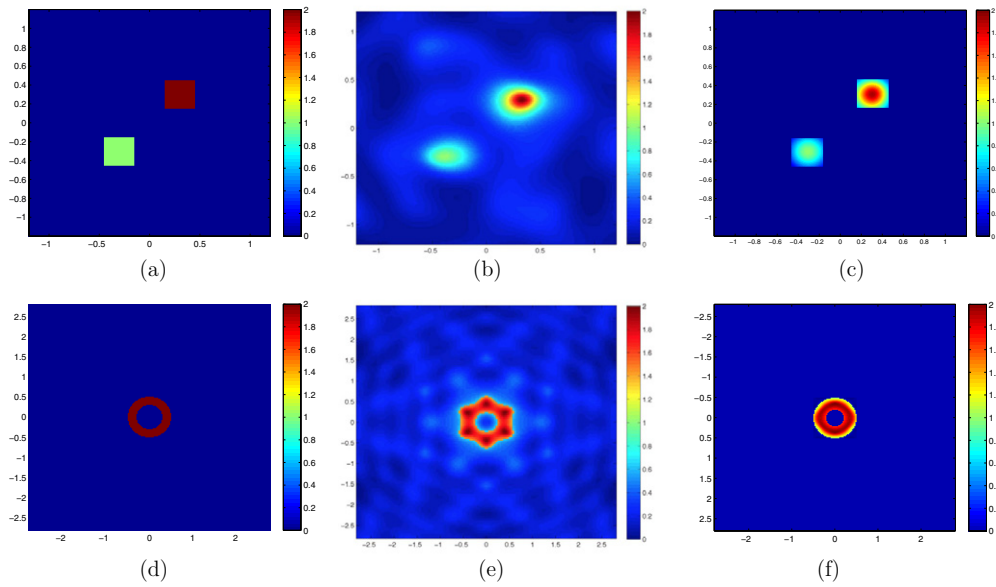
13

Figure 9. True scatterer for (a) example 1 and (d) example 3. The reconstructions by ESCI applied to the originally selected computational region for (b) example 1 and (e) example 3. The reconstructions by ESCI applied to the domain provided by the multilevel sampling algorithm for (c) example 1 and (f) example 3.

may have to take a much larger sampling domain than the actual size of the inhomogeneous media for these methods, so they can be extremely time consuming, especially in three dimensions. Using the newly proposed multilevel algorithm in section 4, we can first locate a much smaller sampling domain than usual (or the one we originally selected) in a numerical reconstruction for the contrast χ. Then we can apply any existing reconstruction algorithms for more accurate reconstructions, starting with an initial sampling domain provided by the multilevel algorithm. This may save us a great fraction of the entire computational costs. Based on above few observations, we think that there is a significant advantage to applying an optimization-type method to the domain achieved by the multilevel sampling algorithm. For comparison, we show some numerical tests using the popular extended contrast source inversion (ECSI) method [18] and the newly proposed multilevel method combined with ECSI.

We consider the same scatterer Ω and the setups as in examples 1 and 3 of section 5.1; see figures 9(a) and (d). Then we apply the ECSI method [18] with mesh size $h = 0.015\lambda$, respectively, to the originally selected computational regions and the reconstructed domains (cf figures 3(d) and 6(d)) by the multilevel algorithm. The reconstructions are shown in figures 9(b), (c), (e) and (f). The four figures are the inverted images of ECSI when it is terminated at the relative L^2-norm error $\epsilon = 10^{-2}$ of the reconstructed contrast values. Clearly, figures 9(c) and (f) give much better reconstructions than figures 9(b) and (e), with quite satisfactory reconstructions of both locations and contrast values. Figure 10 shows the convergence curves in terms of the relative L^2-norm errors against the number of iterations. It is obvious that the ECSI with the help of the multilevel algorithm gives more accurate reconstructions, and with much less computational effort.
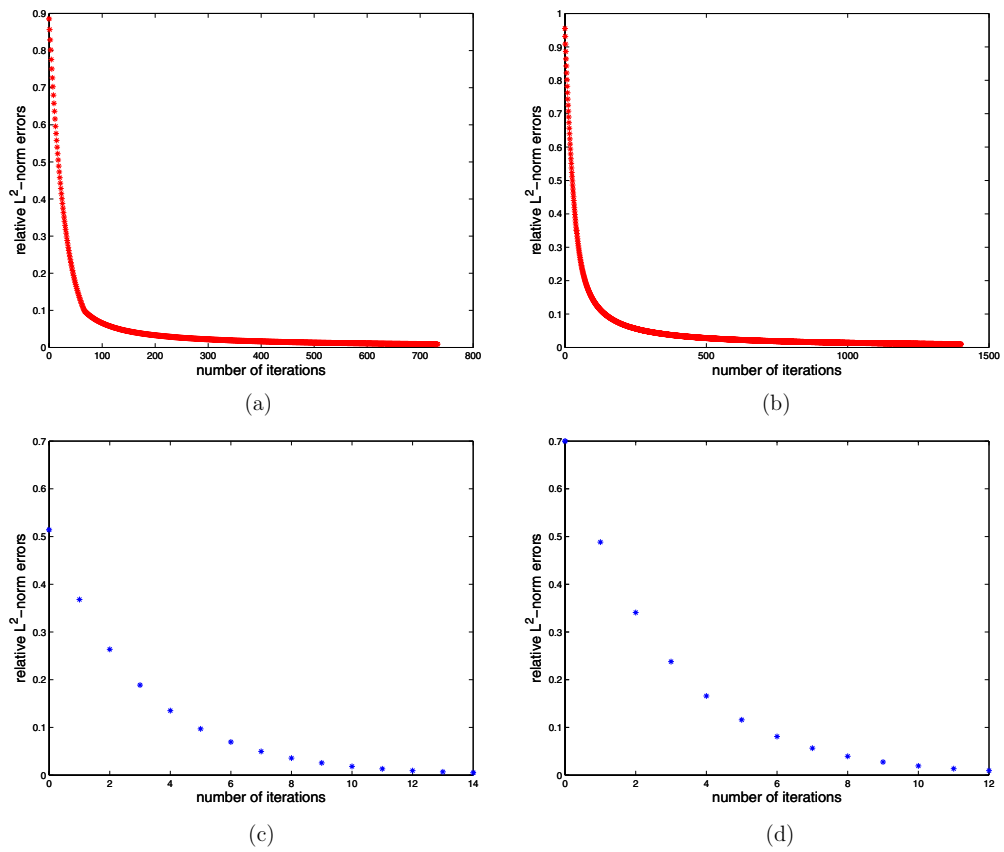
Figure 10. Convergence curve by ECSI applied to the originally selected computational region for (a) example 1 and (b) example 3. Convergence curve by ECSI applied to the domain achieved from the multilevel sampling algorithm for (c) example 1 and (d) example 3.
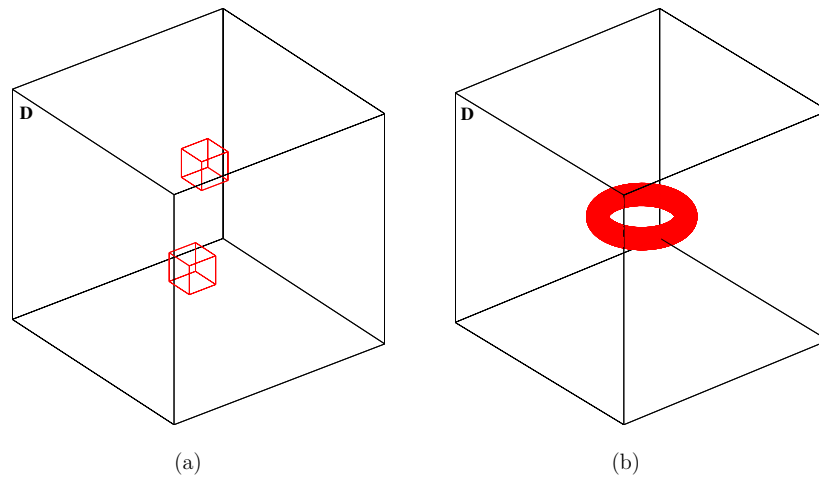

Figure 11. Scatterers imbedded in a large sampling domain: (a) two cubic components close to each other in example 6; (b) a torus in example 7.
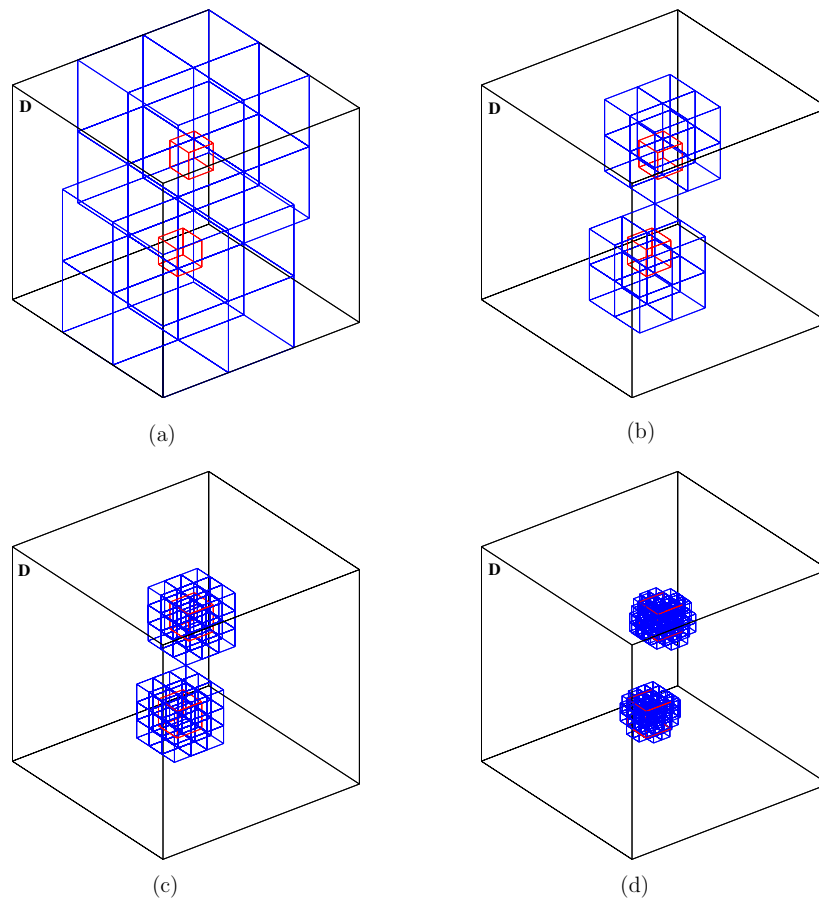
Figure 12. Numerical reconstructions by the first fourth iterations for example 6.

5.3. Three-dimensional reconstructions

Example 6. This example tests a three-dimensional scatterer Ω consisting of two small cubic components,

$$\Omega_1 = [-0.45\lambda, -0.15\lambda]^3, \quad \Omega_2 = [0.15\lambda, 0.45\lambda]^3.$$

The two squares are quite close to each other, both with constant contrast values 2; see figure 11(a). We take the sampling domain to be $\mathbf{D} = [-1.2\lambda, 1.2\lambda]^3$, which is about 500 times of the volume of Ω_1 or Ω_2.

We take an initial mesh size of $h_0 = 0.8\lambda$ in the multilevel algorithm. The mesh refinement during the multilevel algorithm is carried out based on the bisection rule, namely $h_k = 0.8\lambda/2^k$, where k is the kth refinement, and h_k is the mesh size after the kth refinement. The numerical reconstructions are shown in figure 12. As for the previous two-dimensional examples, the reconstructions are quite satisfactory and accurate locations for the scatterer can be achieved, and two inhomogeneous medium objects can be quickly separated. From table 4, we can see more detailed information on the number of grid points that remained or were removed after each iteration of the multilevel algorithm.
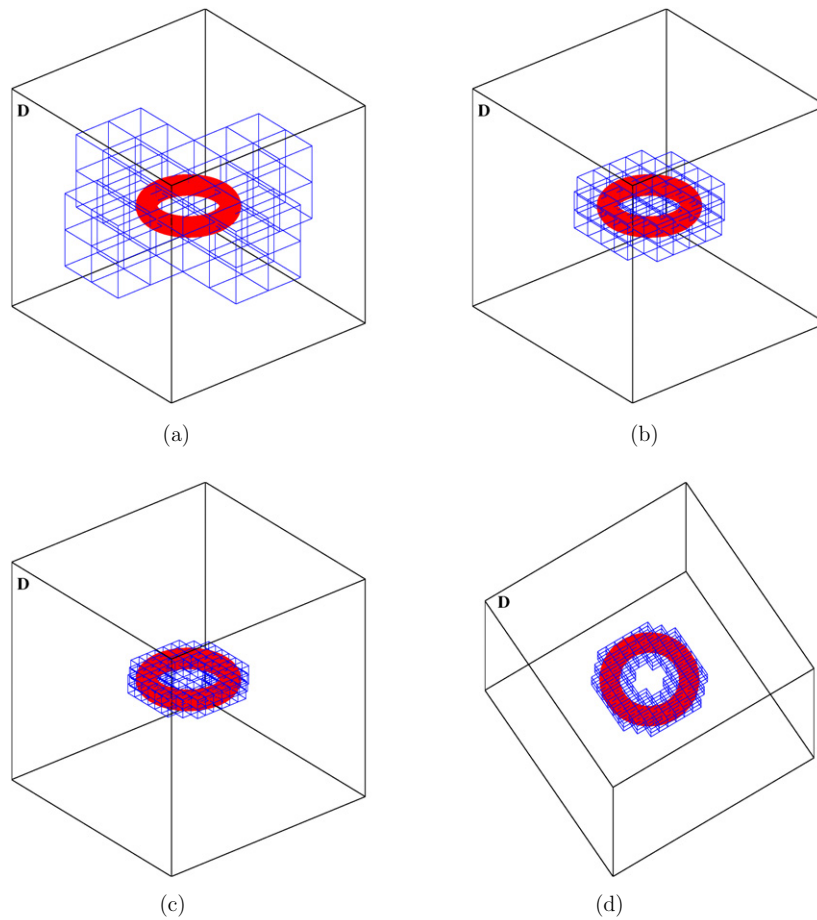
(a)   (b)

(c)   (d)

Figure 13. Numerical reconstructions by the first three iterations for example 7; (d) is the same as (c), but viewed from a different angle.

Table 4. Information about the grid points at each iteration for example 6.

Iteration	1	2	3	4
Number of removed grid points	18	170	122	287
Number of remaining grid points	46	53	127	398
Number of total grid points	64	223	249	685

Example 7. In this test, we consider a torus scatterer (see figure 11(b)), with a contrast value 2. The torus has the following representation,

$$(R - \sqrt{x^2 + y^2})^2 + z^2 = r^2,$$

where $r = 0.1\lambda$ and $R = 0.4\lambda$ (R is the radius from the center of the hole to the center of the torus tube, r is the radius of the tube). The sampling domain is taken to be $\mathbf{D} = [-1.2\lambda, 1.2\lambda]^3$, which is about 170 times the volume of the torus.

We take an initial mesh size of $h_0 = 0.4\lambda$ in the multilevel algorithm. The mesh refinement during the multilevel algorithm is carried out based on the rule $h_k = 0.4\lambda/2^k$, where k is the kth refinement, and h_k is the mesh size after the kth refinement. The numerical reconstructions are shown in figure 13. As for the previous two-dimensional examples, the reconstructions are

Table 5. Information about the grid points at each iteration for example 7.

Iteration	1	2	3
Number of removed grid points	244	390	516
Number of remaining grid points	99	135	249
Number of total grid points	343	525	765

quite satisfactory and accurate locations for the scatterer can be achieved. Again, we can find more information from table 5 on the number of grid points that remained or were removed after each iteration of the multilevel algorithm.

6. Concluding remarks

This work proposes a multilevel sampling algorithm which helps to locate an initial computational domain for the numerical reconstruction of inhomogeneous media in inverse medium scatterings. The algorithm is an iterative process which starts with a large sampling domain, and reduces the size of the domain iteratively based on the cut-off values, which are computed adaptively by using the updated contrast source strengths and contrast values at each iteration. The iterative algorithm can be viewed actually as a direct method, since it involves only matrix–vector operations and does not need any optimization process or to solve any large-scale ill-posed linear systems. The algorithm works with very few incident fields and its cut-off values are easy to compute and insensitive to the sizes and shapes of the scatterers, as well as the noise in the data. This is a clear advantage of the algorithm over some popular existing sampling methods such as the linear sampling type methods, where the cut-off values are sensitive to the noise and difficult to choose, and the number of incident fields cannot be small. In addition, the multilevel algorithm converges fast and can easily separate multiple disjoint scattering components, often with just a few iterations to find a satisfactory initial location of each object. Another nice feature of the new algorithm is that it is self-adaptive, that is, it can remedy the possible errors from the previous levels at each current level. With an effective initial location of each object, we may then apply any existing efficient but computationally more demanding methods for the further refinement of the estimated shape of each scattering object as well as for the recovery of the contrast profiles of different media. However, we would like to emphasize that the new multilevel method aims only at weak scatterers. We know from the numerical point of view that it is rather challenging to reconstruct strong scatterers. There is still no efficient method that can successfully tackle this problem, and neither can our multilevel algorithm deal with it. Nevertheless, with the linear sampling method it may still be possible to locate strong scatterers if the number of incidences is sufficient, since it does not involve wave interactions inside and among scatterers.

Appendix. Discretization

In the numerical implementations of the multilevel sampling algorithm proposed in section 4, we have to discretize all the integrals involved. In this appendix, we discuss briefly the

18

numerical discretization of these integrations. We illustrate only the discretizations of the state and field equations (2.5) and (2.6), as all other integrations involved in the algorithm can be approximated similarly. To do so, we divide the domain **D** into smaller rectangular or cubic elements, whose centers are denoted as $\boldsymbol{x}_1, \boldsymbol{x}_2, \ldots, \boldsymbol{x}_L$.

Using the coupled-dipole method or discrete dipole approximation [3, 10], we can discretize (2.5) by

$$w_j(\boldsymbol{x}_l) = \chi(\boldsymbol{x}_l)u_j^{\text{inc}}(\boldsymbol{x}_l) + k^2\chi(\boldsymbol{x}_l)\sum_{n \neq m} A_n g(\boldsymbol{x}_m, \boldsymbol{x}_l)w_j(\boldsymbol{x}_l), \quad l = 1, 2, \ldots, L, \tag{A.1}$$

where A_n is the area or volume of the nth element. Similarly, we can discretize equation (2.6) at every point $\boldsymbol{x} \in S$ by

$$u_j^{\text{sca}}(\boldsymbol{x}) = k^2\sum_{l=1}^{L} A_n g(\boldsymbol{x}, \boldsymbol{x}_l)w_j(\boldsymbol{x}_l) \quad \text{for} \quad j = 1, 2, \ldots, N_i. \tag{A.2}$$

References

[1] Abubakar A and van den Berg P M 2002 The contrast source inversion method for location and shape reconstructions *Inverse Problems* **18** 495–510
[2] Bao G and Li P 2005 Inverse medium scattering for the Helmholtz equation at fixed frequency *Inverse Problems* **21** 1621–41
[3] Belkebir K, Chaumet P C and Sentenac A 2005 Superresolution in total internal reflection tomography *J. Opt. Soc. Am.* A **22** 1889–97
[4] Chen X 2009 Application of signal-subspace and optimization methods in reconstructing extended scatterers *J. Opt. Soc. Am.* A **26** 1022–6
[5] Chen X 2010 Subspace-based optimization method for solving inverse-scattering problems *IEEE Trans. Geosci. Remote Sens.* **48** 42–9
[6] Chew W, Wang Y, Otto G, Lesselier D and Bolomey J 1994 On the inverse source method of solving inverse scattering problems *Inverse Problems* **10** 547–53
[7] Colton D and Kress R 1998 *Inverse Acoustic and Electromagnetic Scattering Theory* 2nd edn (Berlin: Springer)
[8] Ito K, Jin B and Zou J 2012 A direct sampling method to an inverse medium scattering problem *Inverse Problems* **28** 025003
[9] Kirsch A 2002 The MUSIC-algorithm and the factorization method in inverse scattering theory for inhomogeneous media *Inverse Problems* **18** 1025–40
[10] Lakhtakia A 1992 Strong and weak forms of the method of moments and the coupled dipole method for scattering of time-harmonic electromagnetics fields *Int. J. Mod. Phys.* C **3** 583–603
[11] Levy B and Esmersoy C 1988 Variable background Born inversion by wavefield backpropagation *SIAM J. Appl. Math.* **48** 952–72
[12] Li J, Liu H and Zou J 2008 Multilevel linear sampling method for inverse scattering problems *SIAM J. Sci. Comput.* **30** 1228–50
[13] Li J, Liu H and Zou J 2009 Strengthened linear sampling method with a reference ball *SIAM J. Sci. Comput.* **31** 4013–40
[14] Liu K, Xu Y and Zou J 2012 A parallel radial bisection algorithm for inverse scattering problems *Inverse Problems Sci. Eng.* **21** 197–209
[15] Marengo E A, Gruber F K and Simonetti F 2007 Time-reversal MUSIC imaging of extended targets *IEEE Trans. Image Process.* **16** 1967–84
[16] Potthast R 2006 A survey on sampling and probe methods for inverse problems *Inverse Problems* **22** R1–47
[17] van den Berg P M and Kleinman R E 1997 A contrast source inversion method *Inverse Problems* **13** 1607–20
[18] van den Berg P M, van Broekhoven A L and Abubakar A 1999 Extended contrast source inversion *Inverse Problems* **15** 1325–44
[19] van den Berg P M and Abubakar A 2001 Contrast source inversion method: state of art *Prog. Electromagn. Res.* **34** 189–218
[20] Xu Y, Mawata C and Lin W 2000 Generalized dual space indicator method for underwater imaging *Inverse Problems* **16** 1761–76